Automatic recognition of type III solar radio bursts in STEREO/WAVES data for onboard real-time and archived data processing

V. Lobzin, Iver Cairns, A. Zaslavsky

AGU PUBLICATIONS

JGR

Journal of Geophysical Research: Space Physics

TECHNIQUE

10.1002/2013JA019008

Key Points:
- New methods are developed to detect solar type III bursts in the S/WAVES data
- If the number of false alarms is < 10%, the probability to detect is 81%
- The techniques are useful for building solar radio event databases

Correspondence to:
V. V. Lobzin,
v.lobzin@physics.usyd.edu.au

Citation:
Lobzin, V. V., I. H. Cairns, and A. Zaslavsky (2014), Automatic recognition of type III solar radio bursts in STEREO/WAVES data for onboard real-time and archived data processing, *J. Geophys. Res. Space Physics*, *119*, 742–750, doi:10.1002/2013JA019008.

Received 3 MAY 2013
Accepted 11 JAN 2014
Accepted article online 17 JAN 2014
Published online 14 FEB 2014

Automatic recognition of type III solar radio bursts in STEREO/WAVES data for onboard real-time and archived data processing

V. V. Lobzin[1,2], Iver H. Cairns[1], and A. Zaslavsky[3]

[1]School of Physics, University of Sydney, Sydney, New South Wales, Australia, [2]Now at Learmonth Solar Observatory, IPS Radio and Space Services, Bureau of Meteorology, Exmouth, Western Australia, [3]LESIA, Observatoire de Paris, CNRS, Université Pierre et Marie Curie, Université Denis Diderot, Paris, France

Abstract Type III radio bursts are produced near the local electron plasma frequency and/or near its harmonic by fast electrons ejected from the solar active regions and moving through the corona and solar wind. These bursts have dynamic spectra with frequency rapidly falling with time. This paper presents two new methods developed to detect type III bursts automatically in the data from High Frequency Receiver (HFR) of the STEREO/WAVES radio instrument onboard the STEREO spacecraft. The first technique is applicable to the low-frequency band (HFR-1: 125 kHz to 1.975 MHz) only. This technique can possibly be implemented in onboard satellite software aimed at preliminary detection of bursts and identification of time intervals with relatively high solar activity. In the second technique the bursts are detected in both the low-frequency band and the high-frequency band (HFR-2: 2.025 MHz to 16.025 MHz), with the computational burden being higher by 1 order of magnitude as compared with that for the first technique. Preliminary tests of the method show that the performance of the first technique is quite high, $P_{dL} = 72\% \pm 3\%$. The performance of the second technique is considerably higher, $P_{dL+H} = 81\% \pm 1\%$, while the number of false alarms does not exceed 10% for one daily spectrum.

1. Introduction

Type III radio bursts were unambiguously distinguished from other kinds of solar bursts at the end of 1940s, when the first observations were made with a meter-wavelength radiospectrograph [*Wild and McCready*, 1950; *Wild*, 1985]. These bursts are observed over a wide frequency range, 1 GHz to 10 kHz, typically with a rapid decrease in frequency with increasing time [*Suzuki and Dulk*, 1985]. The early interpretation of their high-frequency drift was a source moving outward through the solar corona with a speed of (2-10) $\times$ 10^5 km s^{-1} [*Wild et al.*, 1954]. Later, energetic electrons associated with type III bursts were found in space experiments [*Gurnett and Anderson*, 1976, 1977]. Now it is agreed that type III bursts are generated by mildly relativistic electrons that are most likely accelerated by reconnection in the low solar corona [e.g., *Aschwanden and Benz*, 1997; *Bastian et al.*, 1998]. Type III bursts are commonly observed whenever there is a bright active region on the visible side of the Sun [e.g., *Suzuki and Dulk*, 1985]. Groups of type III bursts are observed at the impulsive phase of solar flares [e.g., *Dulk et al.*, 1985; *Aschwanden and Benz*, 1997]. However, they are also seen at times when there is no activity at other wavelengths [*White*, 2007], most probably as a result of reconnection in relatively complex magnetic configurations. Recently, *Lobzin et al.* [2011] confirmed that type III bursts can even occur when there are no sunspots on the visible solar disk. However, extensive analysis of observations revealed no evidence that the bursts cannot be associated with active regions [*Lobzin et al.*, 2011].

Lobzin et al. [2011] studied the solar cycle variations of the coronal type III burst occurrence rates (T3BOR) and argued that T3BOR can be considered an additional index of solar activity that should be useful in future studies, for instance, for solar cycle predictions and searches for different periodicities in solar activity. For these studies, the daily values of T3BOR were estimated using a technique implemented in the Automated Radio Burst Identification System (ARBIS) [*Lobzin et al.*, 2009, 2010a] and the Learmonth radio spectra. The estimates obtained were also used in the search for hidden Rieger-type periodicities in the T3BOR time series [*Lobzin et al.*, 2012]. The Rieger-type periodicity with a period of 154 days was found first by *Rieger et al.* [1984] in the occurrence of high-energy gamma ray events observed onboard the Solar Maximum Mission. Later it was also found in a number of solar activity indices and other parameters related to the

Sun and interplanetary medium (for references, see, e.g., *Lobzin et al.* [2012]). This periodicity also exists in the T3BOR during the time interval from 22 June 2000 to 31 December 2003, which partially contains the maximum and the declining phase of solar cycle 23 [*Lobzin et al.*, 2012].

For statistical studies of solar activity in the type III radio bursts and for future development of real-time automated prediction of space weather using solar radio data, it is necessary to develop objective, accurate, and efficient numerical methods for classifying solar radio bursts and estimating their parameters from both ground-based and spacecraft radio data. At present, only meter-wavelength type II and type III solar radio bursts can be identified and classified automatically in archived and real-time data provided by the Learmonth and Culgoora observatories [*Lobzin et al.*, 2009, 2010a]. This study presents two new methods for automatic recognition of type III radio bursts in data from the High Frequency Receiver (HFR) of the STEREO/WAVES (S/WAVES) radio instrument onboard the STEREO spacecraft [*Bougeret et al.*, 2008]. It is worth noting that there exist different approaches to automatic recognition of type III bursts in the data. This paper presents techniques which look the most efficient from computational point of view and thus can be implemented in onboard satellite software.

Automatic recognition of type III bursts and other emissions will be useful for building event databases for the STEREO/WAVES (S/WAVES) radio instrument onboard the STEREO spacecraft [*Bougeret et al.*, 2008] and the Radio and Plasma Waves instrument on Solar Orbiter [*Maksimovic et al.*, 2007]. In particular, they may be useful for studying periodicities of solar activity [e.g., *Lobzin et al.*, 2011, 2012] and the relationships between coronal (25–300 MHz) and interplanetary (0.01–10 MHz) type III bursts. In addition, this is an attractive way to optimize telemetry for the FIELDS instrument on the future Solar Probe Plus spacecraft for transmission to Earth.

The paper is organized as follows. The data used in the study are described in section 2. The procedure of data processing and the results obtained are outlined in section 3. Section 4 summarizes the results and gives the conclusions.

2. Data

In the present study, we use archived data from the High Frequency Receiver (HFR) of the STEREO/WAVES (S/WAVES) radio instrument onboard the STEREO spacecraft [*Bougeret et al.*, 2008]. The HFR is a dual sweeping receiver instrument (HFR-1 and HFR-2) that covers a frequency range 0.125–16.025 MHz with 0.05 MHz increments and completes a frequency sweep every 38.8 s. The total frequency range is split into two bands. The low-frequency band (LFB, which corresponds to HFR-1) contains 38 frequencies from 125 kHz to 1.975 MHz and the high-frequency band (HFB corresponding to HFR-2) contains 281 frequencies from 2.025 MHz to 16.025 MHz. The calibration procedure for these data was developed by *Zaslavsky et al.* [2011]. In the current study we use high-resolution uncalibrated data for autocorrelations. The reason for using uncalibrated data is that our primary focus is on a real-time onboard system that will necessarily have only uncalibrated data. Moreover, the results of the recognition procedure described in the present paper should be the same for calibrated and uncalibrated data.

Three daily spectra were analyzed in detail, specifically, those obtained on 20 January, 1 July, and 13 November 2012 by the STEREO-A spacecraft. These 3 days are well separated in time, and the occurrence rate for type III bursts was quite high, 40–50 events per day, thereby allowing one to create a comprehensive set of events for such statistical studies.

3. Data Processing

The recognition of solar radio bursts in a dynamic spectrum can be considered a problem of object recognition in the image obtained by plotting the spectrum in time-frequency coordinates [*Lobzin et al.*, 2009, 2010a]. Unlike the case of usual images, these coordinates are not equivalent. However, various digital image processing techniques can be used successfully, sometimes with minor modification, as was shown earlier for automated recognition of meter-wavelength coronal type II and type III bursts [*Lobzin et al.*, 2009, 2010a].

The problem is essentially statistical due to the unavoidable noise affecting the spectrum acquisition system and the natural variability of solar bursts. Indeed, some rather strong signals are related to electromagnetic interference from the local hardware. Such interference is visible as the bright horizontal lines in Figure 1a,

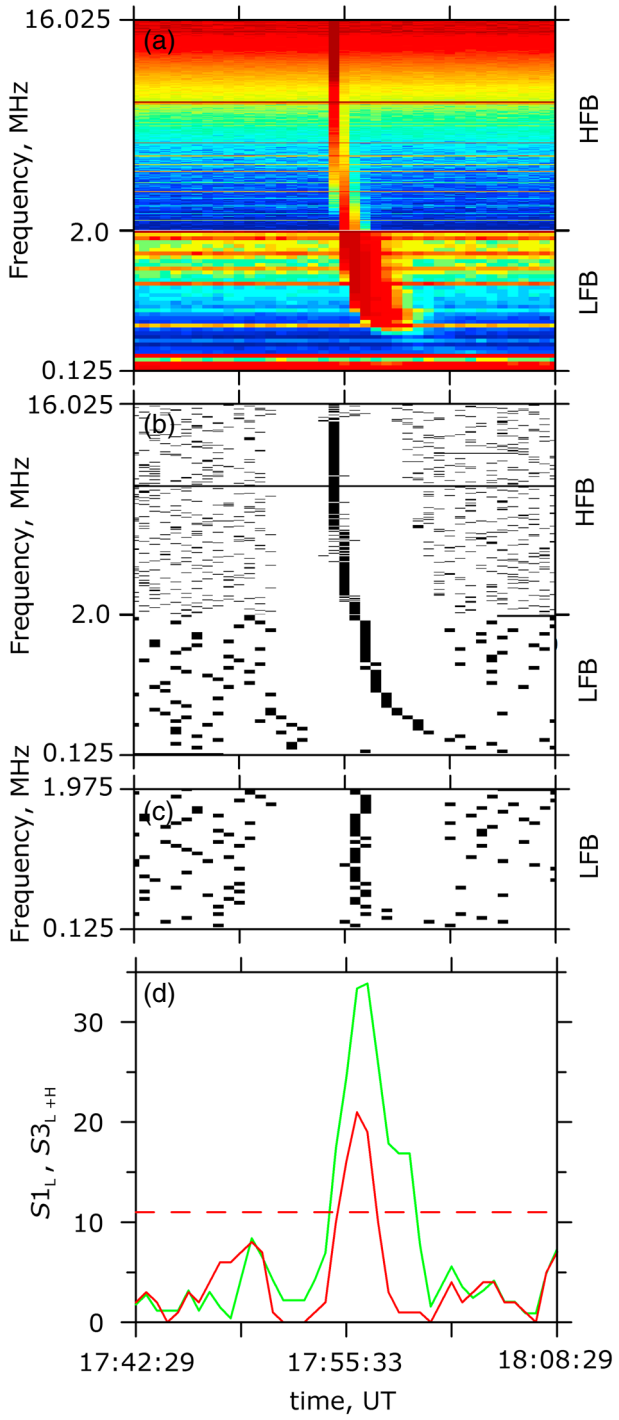

Figure 1. (a) The combined dynamic spectra $G_L(i_t, i_f)$ and $G_H(i_t, i_f)$ of a single type III radio burst observed on 1 January 2012 at 17:56 UT. (b) The corresponding combined binary images $B_L(i_t, i_f)$ and $B_H(i_t, i_f)$. (c) The binary image $B_L(i_t, i_f)$ upon compensation of the typical frequency-dependent delays. (d) Profiles of $S1_L$ (red solid line) and $S3_{L+H}$ (green solid line) versus time and the corresponding threshold levels (dashed lines). In the binary images the pixels are black where $B_{L,H} = 1$ and white for $B_{L,H} = 0$.

which shows an example of a type III burst occupying almost the entire frequency range of the instrument. Another example with a series of relatively weak type III bursts is shown in Figure 2a. In addition, solar type III radio bursts in the frequency range of interest vary in intensity, frequency drift rate, duration, and occupied frequency range, like the meter-wavelength bursts discussed in the review by *Suzuki and Dulk* [1985].

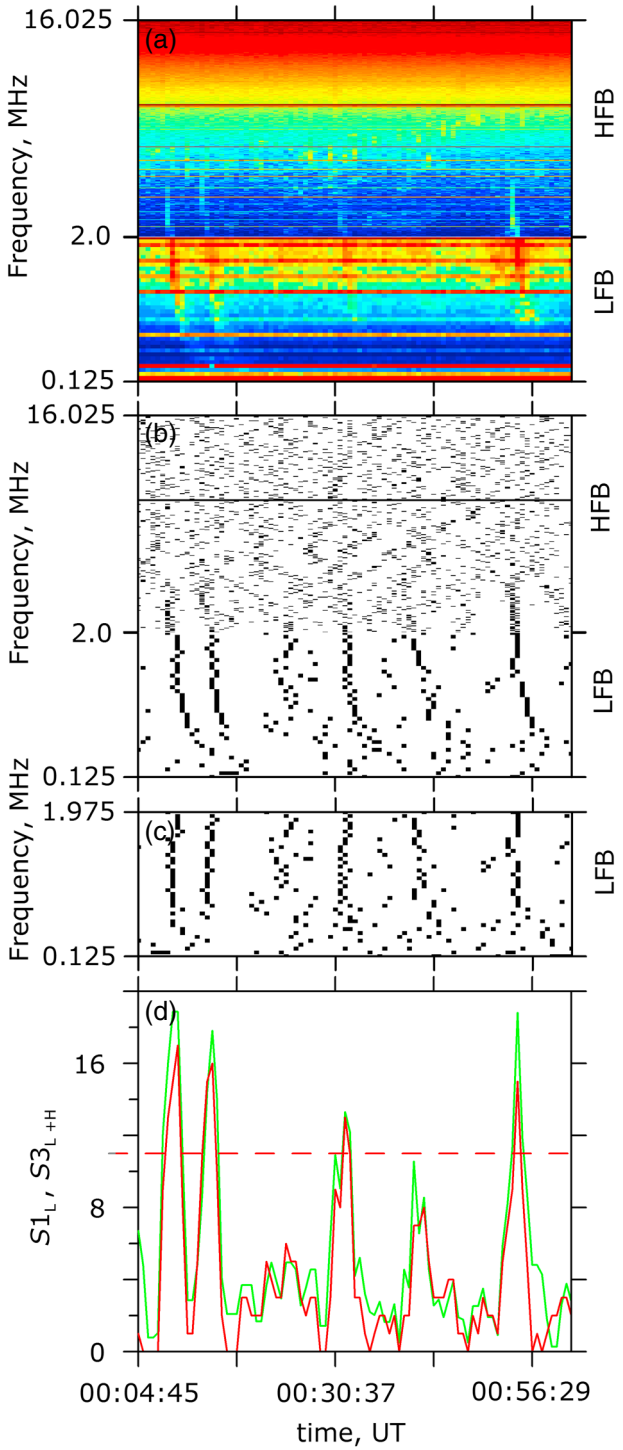

Figure 2. Detection of a series of weak type III bursts. The (a) combined dynamic spectra from 00:04:45 to 01:01:40 UT on 1 July 2012, (b and c) corresponding binary images for the preprocessed spectrum, and (d) profiles of $S1_L$ (red solid line) and $S3_{L+H}$ (green solid line) versus time and the corresponding threshold levels (dashed lines). In the binary images the pixels are black where $B_{L,H} = 1$ and white for $B_{L,H} = 0$.

Suitable procedures for type III burst recognition in S/WAVES data have been found empirically. The processing of the spectra has two stages: preprocessing and recognition.

3.1. Preprocessing

Preprocessing of dynamic spectra is usually required because measured dynamic spectra are not well suited for automated recognition of solar radio bursts. When interpreting data, an automated system is much less flexible than a human operator. This necessitates improving the quality of the picture to be interpreted. In other words, it is desirable to perform an image reconstruction and enhancement aimed at rejecting undesired signals and emphasizing the bursts of interest, thereby increasing the performance of automated detection. On the other hand, preprocessing is also useful for detections by humans as well.

The quality of the images may be relatively low because of several reasons. For instance, if bursts are relatively weak, then strong local interference signals and intrinsic noise may dominate in the measured spectra. On the other hand, usually, data available in near real time, as well as archived data, are not calibrated. In particular, both the effective gain of the receiver and its intrinsic noise may strongly depend on frequency. Indeed, Figures 1a and 2a clearly show that the "background" signal does depend on frequency, the signal being the strongest for the lowest and highest frequencies. The physical signals producing the radio background are known to be due to quasi-thermal noise induced by the local plasma at low frequencies, galactic synchrotron radiation above $\sim$ 500 kHz, and the intrinsic instrumental noise.

The inputs for the first preprocessing procedure are two-dimensional arrays $G_L(i_t, i_f)$ and $G_H(i_t, i_f)$ of the measured dynamic spectra in the low-frequency band and high-frequency band, respectively. Here and in the following, the indices i_t and i_f correspond to time and frequency, respectively, with $i_f = 1, \ldots, 38$ and $i_f = 1, \ldots, 281$ for $G_L(i_t, i_f)$ and $G_H(i_t, i_f)$, respectively. In the arrays $G_{L,H}(i_t, i_f)$, the time intervals between any successive spectra are assumed to be equal to 38.8 s. The index i_t also numbers the measurement times. Because almost all type III bursts in the analyzed spectra manifest themselves as an increase of the measured intensity at the frequency of 1.975 MHz (the highest frequency in the LFB) or slightly less, it is found convenient to take the times of measurements at 1.975 MHz as the time labels for the corresponding sweeps in the spectra $G_L(i_t, i_f)$ and $G_H(i_t, i_f)$.

Typically, object detection in images is computationally intensive. The efficiency can be improved by a suitable transformation of the original gray scale images to the so-called binary images with pixel values 0 or 1 (for brevity, the pixels will be called dark and bright, respectively). The efficiency can be improved further by decreasing the number of bright pixels, specifically, those not likely to be related to the features of interest (type III bursts in this study). Two preprocessing procedures are used to achieve this goal.

The first stage of preprocessing is a moving average filtering of the spectrum image with respect to time. A similar procedure was previously used to find weak coronal type III bursts [*Lobzin et al.*, 2009] and as a part of preprocessing in the ARBIS technique for automatic detection of coronal type II bursts [*Lobzin et al.*, 2010a]. A rectangular window is used for the averaging because of its simplicity. It is worth noting that the very large dynamic range of the signals measured makes it impractical to do such filtering with actual values of the signal. Rather, it is necessary to use the logarithms of the values.

Then, at the second stage, the filtered gray scale image $G_{L,H}(i_t, i_f)$ is converted to a binary image $B_{L,H}(i_t, i_f)$, with pixel values being equal to 1 if there is a significant enhancement in the signal intensity at the corresponding channel and time and 0 otherwise. To decide whether the observed enhancement is significant, it is necessary to choose a criterion. In the present study the criterion is that $B_{L,H}(i_t, i_f) = 1$ if the pixel corresponds to a local maximum with respect to time, i.e., $G_{L,H}(i_t, i_f) \geq G_{L,H}(i_t \pm 1, i_f)$. At the array boundaries corresponding to $i_t = 1$ and $i_t = i_{t\max}$, the definition of the local maximum needs a straightforward modification, i.e., $B_{L,H}(1, i_f) = 1$ if $G_{L,H}(1, i_f) \geq G_{L,H}(2, i_f)$ and $B_{L,H}(i_{t\max}, i_f) = 1$ if $G_{L,H}(i_{t\max}, i_f) \geq G_{L,H}(i_{t\max} - 1, i_f)$. For calibrated data thresholding may be more robust than this simple technique. However, here we use uncalibrated data, as available onboard a spacecraft.

Figures 1a and 2a show an example of type III burst that occupy almost the entire frequency range of the instrument and a series of relatively weak bursts. The final result of such two-stage preprocessing is shown in Figures 1b and 2b (here bright pixels are black while dark pixels are white). Most bright pixels corresponding to the type III bursts are clearly seen and well separated from other bright pixels.

3.2. Recognition

Contrary to spectra preprocessing, the recognition techniques used are not the same for the entire frequency range of the HFR. Rather, examination of the data available and preliminary analysis show that the LFB spectra (125 kHz to 1.975 MHz) should play the leading role in the recognition. The main reason is that the intensity of type III bursts is higher, and most bursts are clearly visible for all frequencies in the LFB, while in the HFB (2.025 MHz to 16.025 MHz) the bursts are typically visible for lower frequencies and then, as the frequency increases, the bursts vanish rather often in the middle of the HFB. Moreover, sometimes the bursts occupy only a few channels in this band, which makes it difficult to successfully apply any statistical procedure for their recognition in the HFB.

Thus, it was concluded that it is worthwhile to develop two different recognition techniques. The first technique is applicable to the LFB only; it has a lighter computational burden because only 38 frequency channels are considered. This technique can possibly be implemented in the onboard software aimed at preliminary detection of the bursts and identification of time intervals with relatively high solar activity, manifested as an increased occurrence rate of type III bursts in the frequency range of interest. On the other hand, in the second technique the bursts are detected in combined LFB and HFB spectra. Although in this case the computational efficiency is also of primary importance, it was found acceptable to increase the computational burden by 1 order of magnitude as compared with that for the first technique, provided the efficiency achieved is considerably higher.

For development and implementation of any recognition technique, it is essential to know the shape of the bursts of interest in the binary images obtained upon preprocessing of the raw spectral data. Examination of the chosen 3 daily spectra shows that the bright pixels corresponding to the intensity maxima of type III bursts in the HFB parts are typically observed in 2–3 adjacent sweeps (see, e.g., Figure 1) and can be approximated by straight lines almost parallel to the frequency axis. Such straight line segments can be detected with the use of Radon transform [*Deans*, 1983], analogously to meter-wavelength type III events observed by solar radio spectrographs belonging to the Radio Solar Telescope Network and Culgoora observatory [*Lobzin et al.*, 2009].

However, for given instrumental time cadence, the curvature of type III traces is substantial at the lower frequencies in the LFB and should be taken into account. Indeed, typically solar type III radio bursts are produced by relatively low-energy electron beams at a speed of about $c/3$, where c is the speed of light. These electrons move along the magnetic field lines away from the Sun and may generate emission near the local plasma frequency and/or near its harmonic [*Suzuki and Dulk*, 1985]. Hence, this emission may be used for probing the local plasma density [see, e.g., *Alvarez and Haddock*, 1973]. Because the plasma density decreases with the distance from the Sun, in type III bursts the maxima observed at lower frequencies are delayed with respect to those at higher frequencies and in the LFB the delay between the lowest and highest frequencies quite often exceeds the duration of 10 sweeps ($\sim$ 6 min).

To take into account this frequency-dependent delay, five events were selected from each daily spectrum and the shape of a typical type III burst observed in the LFB was estimated by median averaging of the delays over this set of 15 events. At the first stage of the recognition procedure the frequency-dependent delays are then compensated using this average shape. If the shape of a burst does not differ considerably from this average shape, then upon compensation its trace in the binary image can be approximated by a straight line almost parallel to the frequency axis (see Figures 1c and 2c), similarly to high-frequency counterparts of typical bursts. It is worth noting that this assumption works better for higher frequencies, where the delays and their uncertainties are smaller, and the optimal procedure need not necessarily take into account data for all frequency channels. Rather, low-frequency channels, where both the delays and their uncertainties are bigger, may be disregarded.

Upon the compensation, the Radon transform is applied to both the HFB and LFB spectra. The Radon transform is approximated by a finite number of sums of the matrix elements $B_{L,H}(i_t, i_f)$ along given segments. For each i_t, in the LFB the segments have the same origin at $(i_t, 38)$, in other words, at the highest frequency in the band, while their ends are at the lowest frequency, $i_f = 1$, and spaced 1 pixel apart in the time direction. The opposite is true for the HFB, where the origins are located at the lowest frequency, $i_f = 1$, while the ends are at the highest frequency, $i_f = 281$. To calculate a pixel value on each segment, the nearest-neighbor interpolation is used. In the LFB, the summation is performed from an $i_{f\,\mathrm{min}} \geq 1$ up to $i_{f\,\mathrm{max}} = 38$, while in the HFB it is done from an $i_{f\,\mathrm{min}} = 1$ up to $i_{f\,\mathrm{max}} \leq 281$. Thereby the matrices $B_L(i_t, i_f)$ and $B_H(i_t, i_f)$ are

Table 1. Type III Bursts Detected in the Data From High Frequency Receiver (HFR) of the S/WAVES Radio Instrument Onboard the STEREO-A Spacecraft[a]

Date	Time (UT)	True Positives For LFB	True Positives For LFB + HFB
20 Jan 2012	0046:07	0	1
20 Jan 2012	0132:30	1	0
20 Jan 2012	0239:07	1	0
20 Jan 2012	0409:00	1	1
20 Jan 2012	0410:57	1	1
20 Jan 2012	0500:06	1	1
20 Jan 2012	0635:49	1	1
20 Jan 2012	0711:23	1	1
20 Jan 2012	0808:57	1	1
20 Jan 2012	0929:09	1	…

[a]This table is available in its entirety in a machine-readable form in the online journal. A portion is shown here for guidance regarding its form and content.

Radon-transformed into matrices $B_{LR}(i_t, i_\tau)$ and $B_{HR}(i_t, i_\tau)$, where the second index i_τ enumerates the displacement of the segments' ends with respect to their origins. It is worth noting that $B_{LR}(i_t, i_\tau)$ and $B_{HR}(i_t, i_\tau)$ also depend on $i_{f\,min}$ and $i_{f\,max}$, respectively.

A maximum value of $B_{LR}(i_t, i_\tau)$ and $B_{HR}(i_t, i_\tau)$ is calculated for each row in the matrices, thereby obtaining two time series $S0_L(i_t) = \max_{i_\tau} B_{LR}(i_t, i_\tau)$ and $S0_H(i_t) = \max_{i_\tau} B_{HR}(i_t, i_\tau)$. Then a background subtraction is performed for the two time series, i.e., $S1_L(i_t) = S0_L(i_t) - S0_{L\,min}(i_t)$ and $S1_H(i_t) = S0_H(i_t) - S0_{H\,min}(i_t)$, where the background values $S0_{L\,min}(i_t)$ and $S0_{H\,min}(i_t)$ are calculated as the minima of $S0_L$ and $S0_H$, respectively, in the vicinity of i_t. Hence, $S1_L(i_t)$ and $S1_H(i_t)$ are nonnegative time series.

In the first technique, to make a decision on whether a type III event is observed in the LFB, the values of $S1_L(i_t)$ are compared with a threshold $S_{L\,threshold}$. When the threshold is exceeded, then this event is considered to be a type III burst.

In the second technique, where spectra for the two frequency bands are processed, it is necessary to take into account that typically the $S1_L(i_t)$ and $S1_H(i_t)$ maxima corresponding to the same event do not have the same i_t. Rather, the peak in $S1_L(i_t)$ is observed later than that in $S1_H(i_t)$ and the delay varies from one event to another. To achieve an approximate synchronism for these peaks, maxima of the series $S1_H(i_t)$ are made wider and shifted to later times, $S2_H(i_t) = \max_{i_t - 5 \le i_t \le i_{t-1}} S1_H(i_t)$. Then the weighted sum of $S1_L(i_t)$ and $S2_H(i_t)$ is calculated, $S3_{L+H}(i_t) = S1_L(i_t) + \alpha S2_H(i_t)$, and compared with a threshold $S_{L+H\,threshold}$, where the parameter α controls the HFB contribution.

The two procedures outlined above use sets of parameters. For the first technique, the set contains a threshold $S_{L\,threshold}$, the length of the "averaging" interval for calculating values of $S0_{L\,min}(i_t)$, and the index $i_{f\,min}$, which determines the lowest frequency taken into account. For the second technique, the set of parameters contains a threshold $S_{L+H\,threshold}$, the pair of indices $i_{f\,min}$ and $i_{f\,max}$, which determine the frequency range taken into account, namely, the lowest frequency in the LFB and the highest one in the HFB, the length of the "averaging" interval, and the parameter α controlling the HFB contribution. The most important parameters seem to be the two thresholds, $S_{L\,threshold}$ and $S_{L+H\,threshold}$.

To find the best set of the parameters, different criteria for optimality can be used. Probably the most appropriate is the Neyman-Pearson criterion [*Neyman and Pearson*, 1967a, 1967b], which maximizes the probability of detection, P_d, for a given acceptable probability of false alarm, P_{fa}. If P_{fa} is chosen, then P_d can be considered as a measure of performance of a detection technique. To find the relationship between P_d and P_{fa}, a representative set of the 141 type III bursts was created and analyzed. The set is composed of all the bursts that were observed onboard the STEREO-A spacecraft on 20 January (44 bursts), 1 July (46 bursts), and 13 November 2012 (51 bursts).

These 3 days chosen are well separated in time, and the type III bursts occurrence rate was quite high for all these 3 days. The events are listed in Table 1. In accordance with the Neyman-Pearson criterion, in order to find the best set of parameters, it is necessary to specify an acceptable probability of false alarms. We require that the number of false alarms should not exceed 10% for each day. In this case the first technique is able to detect 30, 34, and 38 bursts in these 3 daily spectra. The probability to detect and its uncertainty can be estimated as the average of the 3 daily values for these probabilities and the corresponding standard deviation, thereby giving $P_{dL} = 72\% \pm 3\%$. The second technique reveals 36, 38, and 41 events. Its performance is considerably higher while the uncertainty is smaller than those for the first technique, $P_{dL+H} = 81\% \pm 1\%$.

As an aside, we would like to mention an alternative approach to the correction of frequency-dependent delays. This is to use a generalized Radon transform. Indeed, for coronal type III bursts it was shown that the time-varying frequency of peak emission $f(t)$ is well approximated by a function $f(t) = A(t - t_0)^{-\beta}$ [*Cairns et al.*, 2009; *Lobzin et al.*, 2010b]. The summation could then be performed along such curved segments rather than straight ones. This approach is deferred to future work.

4. Summary and Conclusions

This paper presents new objective methods developed to detect type III bursts automatically in data from the High Frequency Receiver (HFR) of the S/WAVES radio instrument onboard the STEREO spacecraft.

The central idea of the implementation is to use the Radon transform to detect bursts as approximately straight segments, which are parallel to the frequency axis in the high-frequency band of the instrument. In the low-frequency band the Radon transform is applied after approximate compensation of the frequency-dependent delays for the bursts maxima observed at different frequencies.

The first technique is applicable to the LFB only; it has a lighter computational burden because only 38 frequency channels are considered. This technique can possibly be implemented in the onboard software aimed at preliminary detections of the bursts and identifying time intervals with relatively high solar activity manifested itself in the increased occurrence rate of type III bursts in the frequency range of interest. In the second techniques the bursts are detected in combined LFB and HFB spectra. Preliminary tests of the first techniques show that the performance of the current implementation is quite high, $P_{dL} = 72\% \pm 3\%$. The performance of the second technique performance is considerably higher, $P_{dL+H} = 81\% \pm 1\%$. The occurrence probability for false positives for the both techniques does not exceed 10% when the type III burst occurrence rate is quite high, 40–50 events per day.

The two techniques described here should be useful for routine detection and documentation of solar type III radio events observed onboard the STEREO spacecraft, as well as the Ulysses, Wind, Galileo, Cassini, and BepiColombo spacecraft. It is particularly relevant to the future Solar Orbiter and Solar Probe Plus missions, for which telemetry optimization is particularly important. Type II bursts and planetary radio emissions are targets for future work. Significantly, modified techniques may be necessary for such emissions due to their different characteristics, as found by *Lobzin et al.* [2009, 2010a] for coronal type II and type III bursts. As well as providing robust ways to limit spacecraft telemetry, the automatic detection techniques in this paper and future work will lead to lists of solar bursts found in the extensive spacecraft data sets. These will facilitate statistical studies of different aspects of solar activity and space weather/climate events, including different hidden periodicities, the approach to solar maximum and minimum, and the connections between interplanetary and coronal radio events.

Acknowledgments
The University of Sydney authors thank the Australian Research Council for funding.

Philippa Browning thanks Milan Maksimovic and an anonymous reviewer for their assistance in evaluating this paper.

References

Alvarez, H., and F. T. Haddock (1973), Solar wind density model from km-wave type III bursts, *Sol. Phys.*, *29*, 197–209.
Aschwanden, M. J., and A. O. Benz (1997), Electron densities in solar flare loops, chromospheric evaporation upflows, and acceleration sites, *Astrophys. J.*, *480*, 825–839.
Bastian, T. S., A. O. Benz, and D. E. Gary (1998), Radio emission from solar flares, *Annu. Rev. Astron. Astrophys.*, *36*, 131–188.
Bougeret, J., et al. (2008), S/WAVES: The radio and plasma wave investigation on the STEREO mission, *Space Sci. Rev.*, *136*, 487–528.
Cairns, I. H., V. V. Lobzin, A. Warmuth, B. Li, P. A. Robinson, and G. Mann (2009), Direct radio probing and interpretation of the Sun's plasma density profile, *Astrophys. J.*, *706*, L265–L269, doi:10.1088/0004-637X/706/2/L265.
Deans, S. R. (1983), *The Radon Transform and Some of Its Applications*, John Wiley, New York.
Dulk, G. A., D. J. McLean, and G. J. Nelson (1985), Solar flares, in *Solar Radiophysics*, edited by D. J. McLean and N. R. Labrum, pp. 53–88, Cambridge Univ. Press, Cambridge, U. K.
Gurnett, D. A., and R. R. Anderson (1976), Electron plasma oscillations associated with type III radio bursts, *Science*, *194*, 1159–1162.
Gurnett, D. A., and R. R. Anderson (1977), Plasma wave electric fields in the solar wind: Initial results from Helios 1, *J. Geophys. Res.*, *82*, 632–650.
Lobzin, V. V., I. H. Cairns, P. A. Robinson, G. Steward, and G. Patterson (2009), Automatic recognition of type III solar radio bursts: Automated Radio Burst Identification System method and first observations, *Adv. Space Res.*, *7*, S04002, doi:10.1029/2008SW000425.
Lobzin, V. V., I. H. Cairns, P. A. Robinson, G. Steward, and G. Patterson (2010a), Automatic recognition of coronal type II radio bursts: The Automated Radio Burst Identification System method and first observations, *Astrophys. J.*, *710*, L58–L62, doi:10.1088/2041-8205/710/1/L58.
Lobzin, V. V., I. H. Cairns, P. A. Robinson, A. Warmuth, G. Mann, R. V. Gorgutsa, and V. V. Fomichev (2010b), Evidence for gently sloping plasma density profiles in the deep corona: Type III observations, *Astrophys. J.*, *724*, 1099–1107.
Lobzin, V., I. H. Cairns, and P. A. Robinson (2011), Solar cycle variations of the occurrence of coronal type III radio bursts and a new solar activity index, *Astrophys. J.*, *736*, L20, doi:10.1088/2041-8205/736/1/L20.
Lobzin, V. V., I. H. Cairns, and P. A. Robinson (2012), Rieger-type periodicity in the occurrence of solar type III radio bursts, *Astrophys. J.*, *754*, L28, doi:10.1088/2041-8205/754/2/L28.

Maksimovic, M., et al. (2007), A radio and plasma wave experiment for the Solar Orbiter mission, in *Proceedings of the 2nd Solar Orbiter Workshop, 16–20 October 2006*, edited by E. Marsch, Athens, Greece, ESA SP-641, Noordwijk, Netherlands.

Neyman, J., and E. S. Pearson (1967a), On the use and interpretation of certain test criteria for purposes of statistical inference: Part I, in *Joint Statistical Papers*, edited by J. Neyman and E. S. Pearson, pp. 1–66, Cambridge Univ. Press, Cambridge, U. K.

Neyman, J., and E. S. Pearson (1967b), The testing of statistical hypotheses in relation to probabilities a priori, in *Joint Statistical Papers*, edited by J. Neyman and E. S. Pearson, pp. 186–202, Cambridge Univ. Press, Cambridge, U. K.

Rieger, E., G. H. Share, D. J. Forrest, G. Kanbach, C. Reppin, and E. L. Chupp (1984), A 154-day periodicity in the occurrence of hard solar flares?, *Nature*, *312*, 623–625.

Suzuki, S., and G. A. Dulk (1985), Bursts of type III and type V, in *Solar Radiophysics*, edited by D. J. McLean and N. R. Labrum, pp. 289–332, Cambridge Univ. Press, Cambridge, U. K.

White, S. M. (2007), Solar radio bursts and space weather, *Asian J. Phys.*, *16*, 189–207.

Wild, J. P. (1985), The beginnings, in *Solar Radiophysics*, edited by D. J. McLean and N. R. Labrum, pp. 3–17, Cambridge Univ. Press, Cambridge, U. K.

Wild, J. P., and L. L. McCready (1950), Observations of the spectrum of high-intensity solar radiation at metre wavelengths. I. The apparatus and spectral types of solar burst observed, *Aust. J. Sci. Res. A*, *3*, 387–398.

Wild, J. P., J. A. Roberts, and J. D. Murray (1954), Radio evidence of the ejection of very fast particles from the Sun, *Nature*, *173*, 532–534.

Zaslavsky, A., N. Meyer-Vernet, S. Hoang, M. Maksimovic, and S. D. Bale (2011), On the antenna calibration of space radio instruments using the galactic background: General formulas and application to STEREO/WAVES, *Radio Sci.*, *46*, RS2008, doi:10.1029/2010RS004464.